Experimental measurement of the C II *L*-shell photoabsorption spectrum

P. Nicolosi and P. Villoresi

Laboratorio di Elettronica Quantistica–Departimento di Electronica e Informatica,
Università di Padova and Istituto Nazionale per la Fisica della Materia, Via Gradenigo 6/A, 35131 Padova, Italy

(Received 22 May 1998)

The photoabsorption spectrum of the C II ion has been experimentally observed using the technique of the two-laser generated plasmas. In this way, both the discrete spectrum, with the series of resonance lines converging to the ionization threshold, and the photoionization cross section above the first limit have been measured. Beyond the threshold the cross section shows several resonances corresponding to ^2S and ^2D open channels and lines corresponding to ^2P closed channels.
[S1050-2947(98)00712-4]

INTRODUCTION

In this paper we present an experimental measurement of the photoabsorption spectrum from the ground state of C II between 38 and 70 nm. In particular, the absorption from the $1s^2 2s^2 2p$ $^2P^o$ ground level, giving rise to the resonance series ns ^2S and nd ^2D, has been measured up to the common ionization limit, at about 50.8 nm. Beyond this, the photoionization continuous spectrum has been observed and several resonances have been resolved.

Carbon is one of the most abundant elements in nature and for this reason it is very important to have a full knowledge of its atomic parameters: energy levels, oscillator strengths, cross sections, etc. In fact, from accurate observations of C spectra it is possible to derive, through spectroscopic analysis, important parameters of the physical environment. For example, C spectra are prominent in radiation emitted by many astrophysical sources as well as in the spectra recorded in various laboratory experiments.

For these reasons carbon spectra have been studied for a long time both theoretically and experimentally. Among the various works reported in the literature the study performed within the framework of the Opacity Project deserves mentioning [1,2]. In particular, Yan and Seaton and Yan, Taylor, and Seaton calculated atomic data for the oscillator strengths and the photoionization cross section of C II by using close-coupling methods. The theoretical prediction of the photoinization cross section of C II has been more recently revised by Lan *et al.* [3]; the authors made a comparison between the results obtained with close-coupling calculations and the UCL package and opacity codes, while oscillator strengths were formerly calculated, particularly those of the resonant transitions $2p$-ns,nd by McEachran and Cohen [4]. On the other hand, extensive experimental measurements are missing; consequently, this cannot allow a deep exhaustive knowledge of the atomic parameters, so the accuracy of theoretical data can be based on comprehensive checks for internal self-consistency as well as on a comparison with other independent calculations.

One well-established technique for the study of atomic spectra is absorption spectroscopy. However, whereas various experiments have been performed with the purpose of measuring atomic parameters for neutral atoms, very few experimental data are reported concerning the matter in ionized states. This is mainly related to the difficulty of generating a suitable absorbing medium, i.e., a column of ions with selected charge and energy state. In fact, energy has to be spent to ionize matter, but unfortunately an ion in a plasma tends to recombine and/or ionize rapidly, so the energy should be supplied in a relatively short time and in a suitable amount, in order to selectively ionize one or a few charge states. In this context the laser produced plasma was recognized as an appropriate source of ions; laser energy, focused onto solid targets, ionizes the matter generating a plasma cloud of high temperature, of the order of hundreds of eV, and high density, typically the critical density for the laser wavelength near the laser-matter interaction layer, which expands rapidly in vacuum. The tendency of the different ion species to separate in both time and space is noteworthy. In fact, the various ionization stages of the elements composing the target appear in the plasma and show different time evolution and spatial distributions because of the fast expansion due to the very high pressure [5]. The higher charge states tend to appear very early in the process and their typical time scales are comparable to the duration of the laser pulse, i.e., a few tens of nanoseconds, while those with lower charge are formed later and last longer. In addition, the former are preferentially confined in the middle region of the plasma cloud; the latter spread out in a wider cone. For these reasons, by varying the laser power density on the target and probing the plasma at a suitable distance from the target, after a proper delay a selected charge state can be found to be favorably populated.

At this point the problem is to irradiate that region of the plasma, at the right time, for the right duration, to get the absorption we are looking for. The laser produced plasma resulted again a suitable source of radiation for accomplishing this task. When the laser pulse is focused on a target of relatively high atomic number element, the generated plasma emits radiation in the vacuum ultraviolet to extreme ultraviolet range in pulses of similar duration to that of the laser pulse, with smooth spectral distribution. This source is essentially pointlike, corresponding to the laser-target interaction region, and consequently has a very high brightness.

In this paper we report the experimental measurement of the absorption spectrum of ionized carbon performed with the dual laser plasma technique. This technique has been
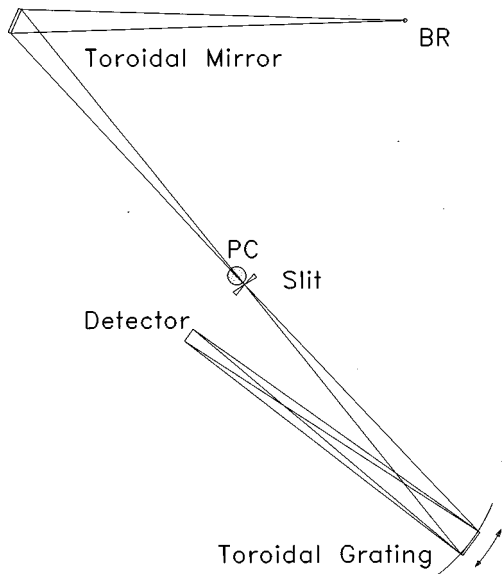
FIG. 1. Scheme of the experiment.   BR, back-radiator plasma; PC, absorbing plasma column.

already applied by our group to study the absorption spectra of multiply charged ions [6,7].

EXPERIMENT

The experiment will be described in detail elsewhere; here we would like to give the essential elements useful for a complete understanding of the measurement. In Fig. 1 a scheme of the experiment is shown. The beam (5 J, 18 ns) from a Nd:YAG laser (where YAG denotes yttrium aluminum garnet) (Q switched and injection seeded for the single longitudinal mode operation) has been split into two parts. About 3.8 J of the laser pulse energy has been sharply focused, using a best form spherical lens ($f=100$), onto a tungsten (W) target generating the back-radiator (BR) plasma. The remaining energy, 1.2 J, has been focused onto a graphite (G) plane target in order to generate the absorbing plasma column.

The W plasma was stigmatically imaged onto the entrance slit of a normal incidence spectrograph via a toroidal mirror

($R=1259.8$ mm, $r=1040.7$ mm, Pt coated, working at angle of incidence 24.6 °). The W target was oriented 45 ° with respect to both the incoming laser beam and the line of sight of the spectroscopic apparatus. In this way the image of the high-density, high-temperature laser-target interaction region, corresponding to the brightest emitting plasma, was projected onto the slit. The G target was placed in front of and close to (about 6 mm from) the entrance slit of the spectrograph. Its surface was oriented perpendicular to the length of the slit; consequently, only a small portion of the expanding G plasma was irradiated by the BR plasma. The size of the probed region was about 0.35 mm wide parallel to the target surface, while along the slit it was defined by the imaging properties of the spectrograph and by the characteristics of the detector. In addition, by moving the target it was possible to probe the plasma in different regions and the time of the probing has been suitably optimized, delaying the generation of the W plasma by varying the length of an optical delay line. Finally, the laser beam has been focused on the G target with a spherocylindrical lens to obtain an elongated plasma column (focal spot 0.1×7 mm^2) increasing the length of the absorbing medium.

The spectrum has been analyzed via a normal incidence stigmatic spectrograph, mounting a toroidal grating ($R=1011.1$ mm, $r=991.8$ mm, Pt coated) of 3600 l/mm. The detector was a two-dimensional charge coupled device (512×512 square pixels of 24 μm with an UV-enhanced response and 16-bit readout, supplied by Princeton Instrument). It was operated at -30 °C, which was the best compromise to get a low thermal noise and a negligible reduction of detection efficiency due to contaminant layer condensation on the detector surface. It was mounted in a fixed position on the focal Rowland surface of the spectrograph. The corresponding dispersion was 6.6 pm/pixel, so about a 3-nm spectral interval was recorded for each exposure. The spectrum was scanned by moving the grating, which was mounted on a rotating arm, pivoted at the center of the Rowland circle and whose length was equal to the radius of the latter. By choosing the grating radii the best stigmatic focusing was obtained in an interval of about 30 nm centered at 56 nm, with an angle of incidence of about 12°. It has been
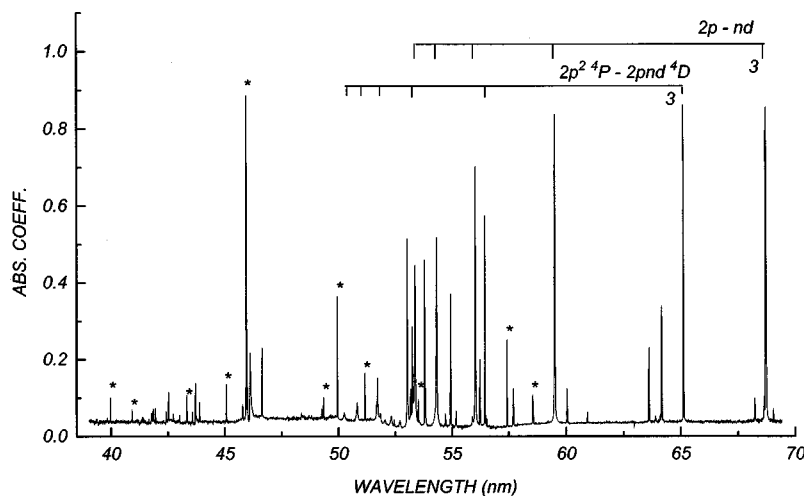
FIG. 2. C II absorption coefficient taken 2.3 mm from the G target and with a delay of 58 ns. Asterisks show C III lines. For further details see the text.

TABLE I. C II transitions to bound states observed and identified, the only high in members of the series.

n	λ_{meas} (nm)	λ_{calc} (nm)
$2s^2 2p\ {}^2P^o - 2s^2 nd\ {}^2D$		
8	52.695	52.700
9	52.320	52.309
10	52.042	52.025
11	51.838	51.816
12	51.672	51.659
$2s2p^2\ {}^4P^o - 2s2p({}^3P^o)ns\ {}^4P^o$		
6	52.455	52.444
$2s2p^2\ {}^4P^o - 2s2p({}^3P^o)nd\ {}^4D^o$		
7	50.820	50.812
8	50.265	50.253
$2s2p^2\ {}^4P^o - 2s2p({}^3P^o)nd\ {}^4P^o$		
7	50.820	50.786
8	50.265	50.236

verified that the residual aberrations allowed about a single-pixel spectral resolution. Although the stigmatic performances of the spectroscopic system have not been fully exploited in the present experiment, they should indeed allow us to record in a single exposure absorption spectra corresponding to different G plasma densities by using an extended source as backlighter. The projection of the pixel size on the plasma corresponds to a magnification of about 1:1, thus defining the size of the probed plasma, as already stated.

In Fig. 2 the spectrum of the absorption coefficient between 38 and 68 nm is reported on a semilogarithmic scale. It was derived by probing the G plasma at about 2.3 nm from the target with a delay of 58 ns between the two laser pulses. About 10–20 laser shot sequences were acquired for each 3-nm spectrally wide exposure and the resulting spectrum is composed of the various adjacent spectral intervals. The C II series starting from the ground state $2p\ {}^2P^o$ and proceeding to the $ns\ {}^2S$ and $nd\ {}^2D$ states is evident. Some C III absorption lines are still present throughout the spectrum, thus showing that the C II population was not completely isolated with respect to other adjacent ionization stages. Indeed, the ionization energy of C II is only 24.38 eV, while that of C I is 11.26 eV. A few other series have been identified in the spectrum, in particular those starting from the first excited level $2p^2\ {}^4P$ and corresponding to transitions to the $2s2p({}^3P^o)nd\ {}^4D$ and ${}^4P$ and $2s2p({}^3P^o)ns\ {}^4P$ states. In Table I the identifications and measured wavelengths corresponding to the high in terms of the observed series are reported. The wavelengths calculated by extrapolating the quantum defect along the series according to the Ritz formula are also reported. The measurements have been derived using some C III or C II lines, already identified and precisely measured [8], as standards. The uncertainty of the wavelength measures has been estimated to be ±0.01 nm due to the discretization of the detector and to the intrinsic spectral broadening of the lines. However, the values have been reported up to ±0.001 nm since the relative position of the lines in the spectrum has been determined with higher accuracy. The two resonance series converge to the common first
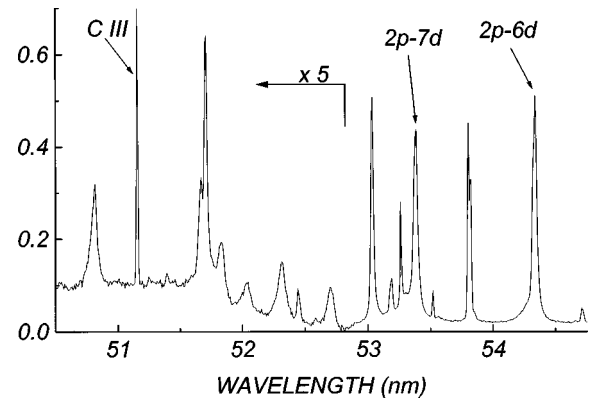
FIG. 3. C II absorption coefficient around the ionization threshold, extracted from Fig. 2. The coefficient of the portion below 52.8 nm has been multiplied by a factor 5 for visualization purposes.

ionization limit $2s^2\ {}^1S$ at about 50.8 nm. In Fig. 3 the enlarged portion of the same spectrum around the photoionization threshold is reported and the absorption coefficient of the shorter wavelength part has been multiplied by a factor 5 for visualization purposes. Here the absorption coefficient has been corrected subtracting a constant value. From the spectrum the effect of strong perturbations of the high-order members, $n \geq 8$, of the two resonance series due to the nearby levels, $({}^3P^o)3p\ {}^2S$ for the ns series and $({}^3P^o)3p\ {}^2D$ for the nd series, is evident. The identification of additional members has been extended up to $n=12$ for the ${}^2D$ series, while the ${}^2S$ series has been clearly followed up to $n=6$, with the member corresponding to $n=7$ merged with the wing of a C III strong line. From the measurement of the absorption coefficient of the $2p$-nd resonance lines, through the correspondingly calculated f values, we expect to derive, with dedicated measurements, the density of C II ions on the ground level and then a measure of the C II photoionization cross section.

Beyond the ionization threshold $2s^2\ {}^1S$ and below the second limit $2s2p\ {}^3P^o$, several resonances appear, showing the typical Fano profiles. This portion of the spectrum is shown enlarged in Fig. 4. The photoionization continuous spectrum in this energy range corresponds to the transitions $2s^2 2p\ {}^2P^o - 2s^2\ {}^1S + \epsilon d\ {}^2D, \epsilon s\ {}^2S$; consequently, according to the selection rules, $({}^1S)ks\ {}^2S$ and $({}^1S)kd\ {}^2D$ are
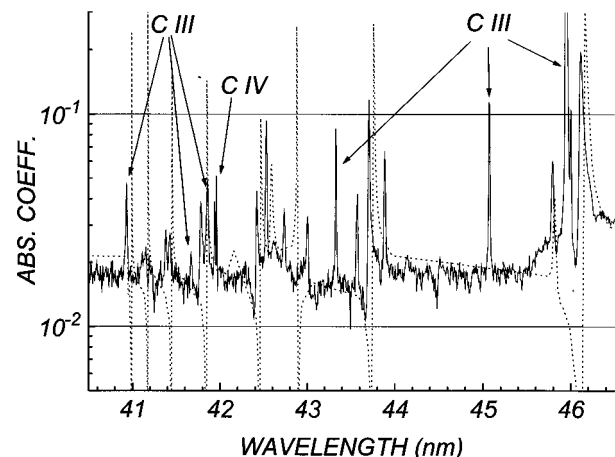
FIG. 4. C II absorption coefficient beyond the ionization threshold, extracted from Fig. 2. The superimposed dotted curve is the theoretical calculation from Ref. [2] scaled for a line density of 5×10^{15} cm^{-2}.

TABLE II. Lines observed beyond the first C II ionization threshold and preliminary assignments.

λ_{meas} (nm)	λ_{calc} (nm)	Configuration
46.650		$2s^22p\ ^2P^o-2s2p(^3P^o)4p\ ^2P$
46.112		$2s^22p\ ^2P^o-2s2p(^3P^o)4p\ ^2D$
45.800		$2s^22p\ ^2P^o-2s2p(^3P^o)4p\ ^2S$
43.886		$2s^22p\ ^2P^o-2s2p(^3P^o)5p\ ^2P$
43.710		$2s^22p\ ^2P^o-2s2p(^3P^o)5p\ ^2D$
43.574		$2s^22p\ ^2P^o-2s2p(^3P^o)5p\ ^2S$
43.008		$2s^22p\ ^2P^o-2s2p(^1P^o)3p\ ^2D$
42.735	42.752	$2s^22p\ ^2P^o-2s2p(^3P^o)6p\ ^2P$
42.630		$2s^22p\ ^2P^o-2s2p(^1P^o)3p\ ^2P$[a]
42.528		$2s^22p\ ^2P^o-2s2p(^3P^o)6p\ ^2S$
42.416	42.420	$2s^22p\ ^2P^o-2s2p(^3P^o)6p\ ^2D$
42.31		$2s^22p\ ^2P^o-2s2p(^1P^o)3p\ ^2S$
41.875	41.851	$2s^22p\ ^2P^o-2s2p(^3P^o)7p\ ^2P+$C III
41.794	41.787	$2s^22p\ ^2P^o-2s2p(^3P^o)7p\ ^2D$
41.683		$2s^22p\ ^2P^o-2s2p(^3P^o)7p\ ^2S$[a]$+$C III
41.435	41.421	$2s^22p\ ^2P^o-2s2p(^3P^o)8p\ ^2P$
41.387	41.382	$2s^22p\ ^2P^o-2s2p(^3P^o)8p\ ^2D$

[a]Tentative assignment.

open channels giving rise to series of resonances, while the $(^1S)np\ ^2P$ states correspond to closed channels, i.e., bound states. In Table II the measured wavelengths and the corresponding preliminary identifications are reported. Identifications have been based on the calculations reported in Refs. [1,4,9,10] and, for the higher members of the series, on extrapolation of the quantum defect. In Table II the calculated wavelengths for these lines are reported. It is noticeable that both the ^2P and ^2D series are perturbed, the first one by the $(^1P)3p\ ^2P$ term and the second by the $(^1P)3p\ ^2D$ term. Indeed, a broad and weak line appears at 42.63 nm and could be assigned probably to $2s^22p\ ^2P^o-2s2p(^1P^o)3p\ ^2P$. In Fig. 4 a superposition of the cross section derived from the calculations of Yan and Seaton is shown for comparison, assuming a column density of carbon ions of 5×10^{15} cm^{-2}. In spite of the good agreement on the average continuous absorption, some discrepancy is present among the relative energies of the resonances; however, the predicted shapes appear to approximate quite well the experimental profiles at least for the low members of the series, while for the others one has to take into account the very low value of the absorption, the correspondingly low signal-to-noise ratio, and the finite instrumental resolution affecting mainly the narrowest features. The minima of the absorption features show essentially a null value of the absorption coefficient, at least within the uncertainty of the experimental data.

CONCLUSIONS

The photoabsorption spectrum of the C II ion has been observed with the technique of the two-laser generated plasmas. In this way both the discrete spectrum, with the series of resonance lines converging to the ionization threshold, and the photoionization cross section have been measured. Beyond the threshold the cross section shows several resonances corresponding to ^2S and ^2D open channels and lines corresponding to ^2P closed channels. The absolute measurement of the cross section is in progress.

[1] Yu Yan and M. J. Seaton, J. Phys. B **20**, 6409 (1987).
[2] Yu Yan, K. T. Taylor, and M. J. Seaton, J. Phys. B **20**, 6399 (1987).
[3] Vo Ky Lan, M. Le Dourneuf, N. L. Allard, H. E. Saraph, and W. Eissner, Comput. Phys. Commun. **55**, 303 (1989).
[4] R. P. McEachran and M. Cohen, J. Quant. Spectrosc. Radiat. Transf. **27**, 111 (1982).
[5] P. Villoresi and P. Nicolosi, Hyperfine Interact. **114**, 213 (1998).
[6] P. Nicolosi, E. Jannitti, and G. Tondello, J. Phys. IV **1**, C1-89 (1991).
[7] E. Jannitti, P. Nicolosi, P. Villoresi, and F. Xianping, Phys. Rev. A **51**, 314 (1995).
[8] R. L. Kelly, J. Phys. Chem. Ref. Data **16**, Suppl. 1 (1987).
[9] W. L. Wiese, J. R. Fuhr, and T. M. Deters, J. Phys. Chem. Ref. Data Monograph No. 7 (1996).
[10] K. A. Berrington (private communication).